frontiers | Frontiers in Physics

ORIGINAL RESEARCH
published: 18 July 2022
doi: 10.3389/fphy.2022.895813

Coupled Antibacterial Effects of Plasma-Activated Water and Pulsed Electric Field

Robin Mentheour* and Zdenko Machala*

Division of Environmental Physics, Faculty of Mathematics, Physics and Informatics, Comenius University, Bratislava, Slovakia

In the biomedical applications of cold plasma, the dominant biological effect is most typically attributed to the reactive oxygen and nitrogen species (RONS), while the physical effect of electric fields is sometimes overlooked. Here, we investigated the antibacterial effect of RONS in plasma-activated water (PAW) on the inactivation of *E. coli* bacteria, coupled with a mild 200-nanosecond pulsed electric field (PEF) treatment. By using transient spark discharge plasma in open atmospheric air and closed air reactors, and by adding hydrogen peroxide (H_2O_2) into the PAW, different chemical compositions of RONS were obtained. We measured the time evolution of the concentrations of key species in the PAW post-discharge: nitrites (NO_2^-) and H_2O_2. PAW rich in both NO_2^- and H_2O_2 showed an antibacterial effect, which was enhanced by the PEF, whereas PAW rich in NO_2^- and poor in H_2O_2 showed an enhancement of the antibacterial effect by the PEF only when H_2O_2 was externally added. The presence of sufficient concentrations of both NO_2^- and H_2O_2 optimized the formation of peroxynitrous acid (ONOOH), which caused a strong peroxidation of the cell membranes leading to the cell death, but it also made them more vulnerable to the PEF treatment. The results suggest that the interaction with radicals during the bacteria exposure to PAW leads to an antibacterial effect reinforced by the pulsed electric field, hence showing a synergy of the chemical and physical plasma agents. This opens new perspectives for applications both plasma and PEF areas of research.

Keywords: cold atmospheric plasma (CAP), plasma activated water (PAW), pulsed electric field (PEF), *E. coli* (*Escherichia coli*), antibacterial effect

OPEN ACCESS

Edited by:
Anna Guller,
Macquarie University, Australia

Reviewed by:
Peter J. Bruggeman,
University of Minnesota Twin Cities, United States
Honghua Hu,
Macquarie University, Australia
Isaac Ekoto,
Sandia National Laboratories (DOE), United States

****Correspondence:***
Robin Mentheour
robin.mentheour@gmail.com
orcid.org/0000-0001-8892-1311
Zdenko Machala
machala@fmph.uniba.sk
orcid.org/0000-0003-1424-1350

Specialty section:
This article was submitted to Biophysics, a section of the journal Frontiers in Physics

Received: *14 March 2022*
Accepted: *24 June 2022*
Published: *18 July 2022*

Citation:
Mentheour R and Machala Z (2022) Coupled Antibacterial Effects of Plasma-Activated Water and Pulsed Electric Field. Front. Phys. 10:895813. doi: 10.3389/fphy.2022.895813

1 INTRODUCTION

Pulsed electric fields (PEF) and cold atmospheric plasma biological treatments bring new applications, such as antibacterial sterilization, cancer therapy, improved wound healing, activation of seed germination and plant growth stimulation in agriculture, disinfection and improvement of food quality and shelf-life extension of food products, and water decontamination [1, 2]. PEF and cold plasma have some common mechanisms of action: electropermeabilization and electroporation of cell membranes due to the electric field [3–5] and induced production of intracellular reactive oxygen species (ROS) [6]. Together with pH decrease in water solutions, these effects play important roles in these emerging applications.

The plasma sources used for biological applications are represented by a multitude of atmospheric cold plasmas, among which streamer corona, dielectric barrier discharge (DBD) [1], helium and argon plasma jets [7], glow discharge, guiding arc [8, 9], and transient spark [10, 11] are well described to induce antibacterial effects. They were also demonstrated to be efficient in other applications, such as cancer therapy [7, 12–14], gene transfer [15], plant growth simulation [16], food industry [17], and wound healing [18, 19]. The mechanisms and the importance of individual effects of plasma agents, and their synergies are not completely understood and are being subjected to intense investigations [13]. They depend on plasma source type, geometry, power delivered, gas molecular composition and humidity [20], ambient pressure and temperature, and target type [7].

The main plasma agents responsible of antibacterial properties are UV radiation, electric field, and especially reactive oxygen and nitrogen species (RONS). The UV radiation (UVA–UVB) generated by plasma is usually not energetic enough to directly inactivate bacteria [21], but it is able to generate RONS in air, which are known for their antibacterial activity or can synergize with plasma-generated RONS [22].

RONS are mainly generated by the reactions of free electrons of the plasma or are the by-products of reactions between radicals and other RONS. RONS generated by plasma are usually classified in two categories. First, species with short lifetime (~ns–μs–ms), for example, superoxide ion, such as O_2^-, and radicals, such as $^\bullet OH$, $^\bullet NO$, O•, and H• [23], which are difficult to detect, especially once they are dissolved in a liquid. Once the plasma is turned off, the short lifetime RONS, especially the radicals, rapidly dissipate. The second category are the long lifetime RONS (~s–min–h), such as hydrogen peroxide, H_2O_2; nitrous oxide, NO; nitric oxide, NO_2; and ozone, O_3, which are transported into liquids and form aqueous forms of H_2O_2, O_3, and nitrites and nitrates (NO_2^- and NO_3^-). Gaseous ozone and nitrogen oxides (NOx) can be quantified by infrared spectroscopy [24, 25] and gas chromatography, and some radicals, such as $^\bullet NO$, $^\bullet OH$, and H_2O_2, by laser-induced fluorescence. $^\bullet OH$,$^\bullet OH_2$, and $^\bullet NO$ radicals generated in liquids are also measured using chemical probes, absorption/fluorescence spectroscopy, electron spin resonance spectrometry with specific spin traps [23], or nuclear magnetic resonance spectroscopy [20].

The presence of water in air plasma can significantly influence the plasma-induced gas-phase chemistry. Highly reactive hydroxyl ($^\bullet OH$) radical can be produced by several reactions, for example, by **Eqs. 1**, **2**.

$$e + H_2O \rightarrow e + {}^\bullet OH + {}^\bullet H \quad (1)$$

$$O(1D) + H_2O \rightarrow {}^\bullet OH + {}^\bullet OH \quad (2)$$

The $^\bullet OH$ radicals recombine resulting in further reactive oxygen species (ROS), such as H_2O_2 (**Eq. 3**) and $^\bullet HO_2$ [24, 26].

$${}^\bullet OH + {}^\bullet OH + M \rightarrow H_2O_2 + M \quad (3)$$

The NO and NO_2 gases are generated by gas-phase reactions of plasma-dissociated N_2 and O_2. The $^\bullet NO$ radical was detected in the gas phase and is a precursor of NOx molecules in the gas phase. The $^\bullet OH$ radicals react with plasma formed NOx and other RNS, resulting in HNO_2 (**Eq. 4**) and HNO_3 [9, 11, 24, 27].

$${}^\bullet ON + {}^\bullet OH \rightarrow HNO_2 \quad (4)$$

Water (either deionized or in various water solutions) treated by plasma, so-called plasma-activated water (PAW), receives RONS from the plasma and retains their biophysical activity, such as antibacterial effects, which makes PAW transportable and applicable even after the plasma treatment [8, 9, 12, 23, 24, 28, 29].

The dissolution of species from the gas phase into the liquid phase is driven in the first approximation by Henry's law. The Henry's law solubility coefficient of H_2O_2 ($k_H \approx 10^3$ mol m^{-3} Pa^{-1}) is about 7–8 orders of magnitude larger than that of NO (≈2 × 10^{-5} mol m^{-3} Pa^{-1}) or NO_2 (≈10^{-4} mol m^{-3} Pa^{-1}) or O_3 (≈10^{-4} mol m^{-3} Pa^{-1}). PAW chemical composition depends on the gaseous RONS generated by the plasma source, which are transported in PAW according to their concentrations in gas and liquid, their interface area, and their Henry's law coefficients. Under certain conditions, plasma products accumulate in the air, especially NO and NO_2 gases [28], and dissolve in water [**Eqs 5–7**] while acidifying PAW and generating NO_2^- and NO_3^- in the liquid [10, 29].

$$NO_2\,(aq) + NO_2\,(aq) + H_2O\,(l) \rightarrow NO_2^- + NO_3^- + 2H_3O^+ \quad (5)$$

$$NO\,(aq) + NO_2\,(aq) + H_2O\,(l) \rightarrow 2NO_2^- + 2H_3O^+ \quad (6)$$

$$HNO_2\,(aq) + H_2O\,(l) \rightarrow NO_2^- + 2H_3O^+ \quad (7)$$

The main long-lifetime species measured in PAW are nitrites (NO_2^-), nitrates (NO_3^-), ozone (O_3), and hydrogen peroxide (H_2O_2). The dissolution of NOx (**Eqs 5–7**) and HNO_2 (pK_a [HNO_2/NO_2]=3.4) [3] in PAW are responsible for the presence of nitrites NO_2^-. The Henry's law coefficient of gaseous HNO_2 is several orders of magnitude higher than that of NO and NO_2, which brings the hypothesis that NO_2^- in liquid dominantly comes from HNO_2 rather than from NO + NO_2 dissolution. This was experimentally evidenced in the study mentioned in reference [30]. A reduced pH value (acidity) is also typical in PAW made from non-buffered water solution [10, 28, 29, 31].

In contrast to NOx, H_2O_2 is much more soluble in water than NOx, due to its high Henry's law coefficient. Thus, most of gaseous H_2O_2 is immediately absorbed by the liquid. The measured H_2O_2 in the liquid phase comes dominantly from this dissolution from the air plasma through the plasma–liquid interface, as studied by references [20, 32] and [33]. H_2O_2 is typically one of the main components of PAW and plays a key role in radical production and in the antibacterial effect. A combination of PAW and H_2O_2 was tested on *S. aureus* and led to a significant antibacterial effect in comparison with their individual effects [34].

H_2O_2 reacts with NO_2^- in acidic conditions and produces peroxynitrous acid, ONOOH, (**Eq. 8**) [7, 9, 10, 12, 28] or its ionic form peroxynitrite, $ONOO^-$, [1, 11, 24, 29, 31]. This pH- and temperature-dependent co-destruction of NO_2^- and H_2O_2 brings a competition between NO_2^- and H_2O_2 in PAW and affects the chemical kinetics (**Eq. 9**) [29]. This competition can lead, depending on their original concentrations, to either NO_2^--dominant or H_2O_2-dominant PAW.

$$NO_2^- + H_2O_2 + H^+ \rightarrow ONOOH + H_2O, \quad (8)$$

$$r = \frac{d[O = NOOH]}{dt} = k[NO_2^-][H_2O_2]. \quad (9)$$

The kinetic rate constant of the reaction (**Eq. 8**) is k=1.1 × 10^{-3} M^{-2} s^{-1} at pH 3.3 [28]. Peroxynitrous acid, ONOOH, is considered as a key factor in antibacterial effect of PAW in acidic conditions [10, 24]. Its antibacterial effect was attributed to the degradation products of peroxynitrous acid, which to 30% generates radicals $^{\bullet}NO_2$ and $^{\bullet}OH$ and the other 70% is converted to nitrate NO_3^- [28]. The radical $^{\bullet}OH$ is known to cause lipid peroxidation of the cell membranes.

Direct plasma biomedical effects are typically stronger than indirect (remote) effects of PAW. Reactive species with a short lifetime are the best candidates to explain this difference, but the difficulty in quantifying and producing these species makes it complicated to evaluate their roles in the antibacterial effect [21].

The presence of an electric field is another obvious difference between direct plasma and the PAW treatments. Focusing on the effects of the electric field and their synergy with RONS can help us to advance the understanding of plasma treatments in a broader perspective. Studies of E-field measurements in plasma jets [35–37] applied for plasma medical applications demonstrated that an E-field is an important agent in plasma-induced biological effects. This is the key motivation of this study to study the separate and the combined effects of RONS in PAW and the pulsed electric field.

The PEF application typically leads to permeabilization of the cell membrane, which may be reversible. Increased pulse length, pulse amplitude, and numbers of pulses lead to irreversible electroporation, that is, cell death. The application of electrical pulses sufficient to produce a transient, elevated transmembrane potential of typically 200 mV–1 V is required for the formation of pores, which perforate the membrane and are filled by water molecules (the so-called aqueous or hydrophilic pores). This transmembrane potential charges the membrane due to the ion flow and leads to a rapid, localized rearrangement of the molecular structure of the membrane. In some circumstances, when the external electric field is removed, the membrane recovers [38].

The RONS coming from the plasma can be responsible for membrane phospholipid peroxidation. Especially, $^{\bullet}OH$ radicals oxidize unsaturated bonds of membrane lipids by fragmentation to truncated-chain lipids and fatty aldehydes. This lipid peroxidation facilitates electropermeabilization and electroporation by reducing the membrane thickness, increasing its fluidity, and facilitating the electroporation by a low E-field [39], leading to a drop in the average time needed to initiate electroporation [40] and a lower threshold electric field needed for pore formation [40–44]. In certain cases, lipid peroxidation can produce the formation of pores on the order of 10 nm–1 μm in size [39, 43].

The interactions between PAW and PEF were investigated by several studies, for example, on bacteria [45] and cancer cells [12, 46–48], and gave promising results by improving the effectiveness of each individual method. The study mentioned in reference [49] has shown that corona discharge plasma for the same energy was more efficient than PEF for an antibacterial effect. The permeabilization of the cells induced by the electric pulses facilitated the antibacterial or anticancer effect of the RONS by penetration into the cancer cells [50]. In addition, the effect of pH could affect the resistance of bacteria to the PEF. Gram-positive bacteria are more resistant at pH=7 and weaker at pH=4, while Gram-negative ones are more resistant at pH=4 and weaker at pH=7 [51].

In this study, we exposed *E. coli* in the planktonic form to two different types of PAW, generated by the transient spark discharge with a water electrospray (TS-ES) in open air and transient spark batch water treatment (TS-B) generated in a closed air reactor. TS-ES has been investigated in detail in the precedent works of our group [10, 11, 24], showing strong antibacterial effects for both direct and indirect (PAW) treatment and associated these effects with the gas and liquid phase plasma-induced chemistry. The antibacterial action of TS-B compared with TS-ES and other air discharges treating batch water against uropathogenic infections were studied recently by the study mentioned in reference [52]. In this study, the RONS composition of these two types of PAW were analyzed directly as produced, or was reinforced in the content of hydrogen peroxide by adding H_2O_2 commercial solution of different concentration values. The antibacterial and chemical effects of PAW only, PAW with added H_2O_2, and the coupled effects of PAW + PEF were investigated.

2 METHODOLOGY

We exposed *E. coli* in the planktonic form to two different types of PAW (**Figure 1**), generated by the transient spark discharge with water electrospray (TS-ES) in open atmospheric air and transient spark batch treatment (TS-B) generated in closed air reactor. The antibacterial action of these two types of PAW was tested as they were produced, or were reinforced by adding H_2O_2 commercial solution of different concentration values. The control and H_2O_2 only condition were also tested in the same way as the other PAWs. Bacteria were diluted in the PAW with a ratio of 1:100 (overnight culture: PAW) and incubated for 10 min. A fraction of the incubated bacteria in PAW was sampled and placed in a commercial electroporation cuvette where PEF was applied. The bacteria were not separated from the PAW, and no supplementary liquid was used in the electroporation cuvette. The PEF treatment was applied to the cuvette 2 min after the beginning of the incubation and then all bacteria finished their total 10 min incubation in PAW. Rapid dilutions of the treated bacterial solutions were carried out before being placed in Petri dishes with agar for an overnight incubation.

2.1 Transient Spark in the Batch System in the Closed Air Reactor

Deionized water (DW) is activated by plasma (**Figures 2A,B**) in a 1L cube-shaped plastic reactor. One side of the cube can be removed, what is here called the “Open reactor” condition, or closed, blocking the renewal of gases from the outside ambient air, what we call the “Closed reactor”. In the reactor, DC-driven transient spark (TS) discharge in positive polarity was generated between the high voltage needle and a surface of 5 ml of DW. DW was contained in a 3-cm-diameter glass Petri dish where a ground stainless steel wire ring electrode was immersed on the dish bottom. TS discharge was initiated by a high electric field that

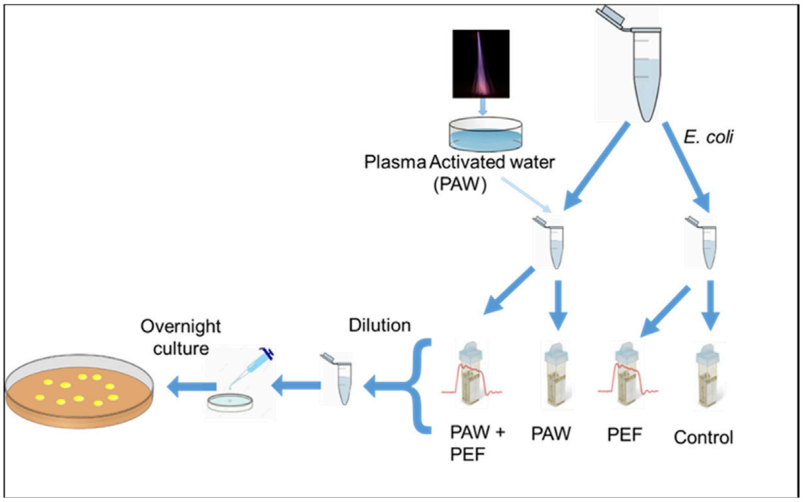

FIGURE 1 | Schematics of the experiment to investigate the antibacterial effect of PEF, PAW, and the coupled PAW + PEF.

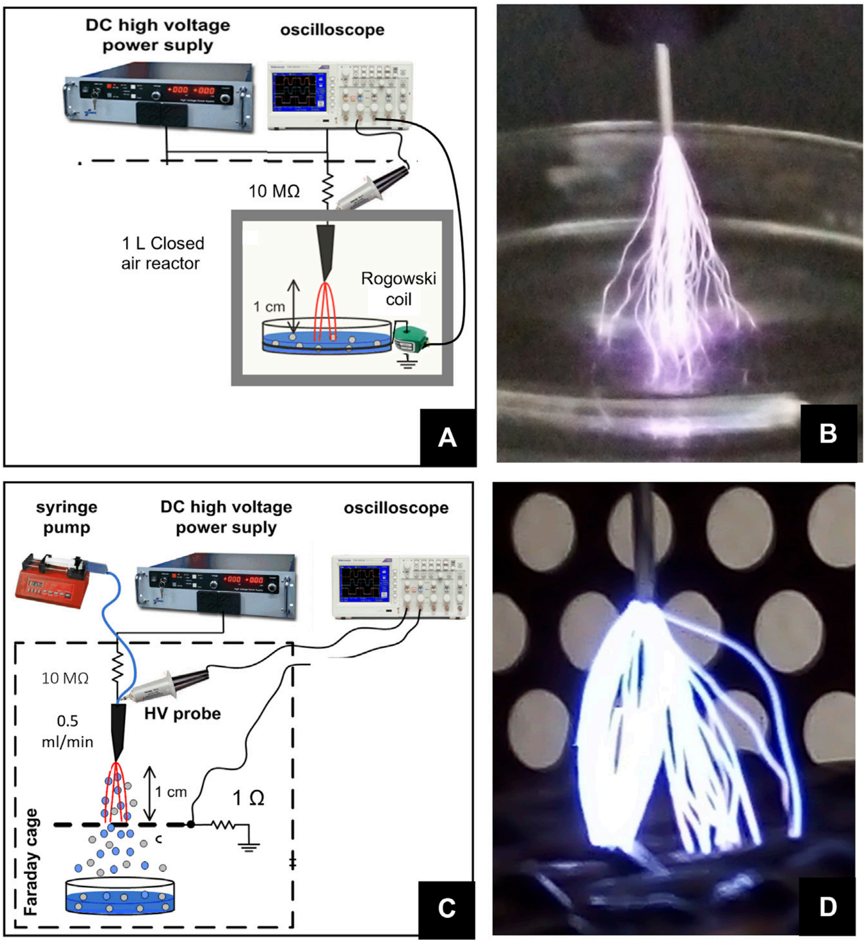

FIGURE 2 | (A) Photo of a typical transient spark discharge in the batch (TS-B) discharge in the closed air reactor. **(B)** Experimental setup of TS-B closed air reactor. **(C)** Photo of a typical transient spark with water electrospray (TS-ES) open air discharge. **(D)** Photo of a typical TS-ES open air discharge.

TABLE 1 | Number of repetitions of *E. coli* antibacterial experiment for the different experimental conditions.

	TS-B		TS-ES	
Experimental condition	CT TS-B	PEF TS-B	CT TS-ES	PEF TS-ES
Number of repetitions	*8*	*4*	*6*	*4*
Experimental condition	TS-B	TS-B + PEF	TS-ES	TS-ES + PEF
Number of repetitions	*8*	*8*	*6*	*6*
Experimental condition	TS-B + 100 µM H_2O_2	TS-B + 100 µM H_2O_2+ PEF	TS-ES + 1 mM H_2O_2	TS-ES + 1 mM H_2O_2 + PEF
Number of repetitions	*4*	*4*	*6*	*6*
Experimental condition	TS-B + 500 µM H_2O_2 + PEF	TS-B + 500 µM H_2O_2 + PEF	TS-ES + 2 mM H_2O_2	TS-ES + 2 mM H_2O_2 + PEF
Number of repetitions	*4*	*4*	*6*	*6*
Experimental condition	TS-B + 1 mM	TS-B + 1 mM H_2O_2 + PEF	TS-ES + 10 mM H_2O_2	TS-ES+ 10 mM H_2O_2 + PEF
Number of repetitions	*3*	*3*	*6*	*6*
Experimental condition	TS-B + 2 mM H_2O_2	TS-B + 2 mM H_2O_2 + PEF		
Number of repetitions	*3*	*3*	*H_2O_2*	
Experimental condition	TS-B + 10 mM H_2O_2	TS-B + 10 mM H_2O_2 + PEF	H_2O_2 only	H_2O_2 +PEF
Number of repetitions	*4*	*4*	*7*	*7*

causes a cascade of ionizations by forming pre-spark streamers, which produce ions and pre-heat the channel. Once the channel is sufficiently conductive, the spark appears through the channel as a strong current peak with the amplitude of 1–3 A and duration of 50–150 ns accompanied by a fast voltage drop. A 10 MΩ ballast resistor was placed in series on the output of the HV generator. The electrical discharge parameters were recorded by a digital oscilloscope *Tektronix TDS 2024C*, the voltage was measured by a high voltage (HV) probe Tektronix P6015A, and the discharge current was measured by a Rogowski coil (Pearson Electronics 2877).

2.2 Transient Spark With a Water Electrospray in Open Air

Plasma-activated water (PAW) in the water electrospray system (**Figures 2C,D**) was created from DW flowing through a high voltage needle placed 1 cm from a metal grid grounded through a 1 Ω resistor. DW was injected directly into the TS discharge by a syringe pump at the flow rate 1 ml/min and electro-sprayed. More details on the TS with the water electrospray system can be found in our previous studies, for example, [10, 24, 53–55] The PAW was collected in a sterile Petri dish under the grid electrode. Voltage was measured at the needle by a HV probe Tektronix P6015A. Maximum voltage was 15 kV. Current was measured as the voltage drop across the 1 Ω resistor between the grid and the ground. TS with DW electrospray in this configuration typically creates the current pulses of 27–30 A. The oscilloscope measured the frequency of the discharge pulses, which is related to the applied voltage. This frequency is maintained at 1 kHz (+/− 200 Hz) by controlling the output voltage of a DC HV generator. A 10 MΩ ballast resistor was placed on the output of the HV generator.

2.3 Bacteria Cultivation

Bacteria suspension of Gram-negative *E. coli* (ATCC 25922) was suspended in water in the planktonic form with an initial population of 10^6 to 10^7 colony forming units per ml (CFU/ ml^{-1}). The suspensions were prepared by the dissolution of bacteria cultivated on sterile liquid nutrient (Lauria–Bertani broth, Biolab). After overnight cultivation (~18 h at 37°C) bacteria were active and vital. The plasma experiments with bacterial suspensions were performed with PAW generated by TS-ES open air discharge and closed air TS-B, both operating in ambient atmospheric air with water electrospray or batch treatment and were repeated 3–10 times. The number of bacteria cells in the suspension was evaluated immediately after plasma treatment by counting CFUs cultivated on agar plates (Lauria–Bertani agar, Biolab) for 16–18 h at 37°C. Just after experiment, bacteria were diluted several times into saline solution (0.85% NaCl) to stop the plasma agents' activity. They were spread on agar plates in Petri dishes and incubated overnight. The standard colony forming unit (CFU) cultivation method was employed. The numbers of repetitions per each type of experiment are presented in **Table 1**.

2.4 Pulsed Electric Field Application

PAW containing the long-lived RONS is subjected to the pulsed electric field (PEF) to investigate the synergic antibacterial effects of PAW and PEF. *E. coli* bacteria in the planktonic form in PAW (or DW for reference) were placed in an electroporation cuvette (VWR 732–1136) with a 2 mm interelectrode distance between the planar aluminum electrodes containing 400 µL of liquid. The applied high voltage from SR20-R-1200 Technix power supply was driven by a low voltage 5 V square signal from a function generator controlling a fast high voltage switch (Behlke HTS 301-03GSM). It allowed for the generation of a sequence of square high voltage pulses of 2.5 kV amplitude and 200 ns duration, applied during 100 s at a frequency of 100 Hz in the electroporation cuvette. The voltage was measured by HV probe Tektronix P6015A, and the discharge current was measured by a Rogowski coil (Pearson Electronics 2877). The electrical characteristics were recorded by oscilloscope Tektronix TDS 2024C.

The conductivity of PAW varies with respect to the DW according to the plasma activation times due to the addition of ions. The conductivity was measured by a conductivity meter [GREISINGER Electronique GMH 3430]. The original DW conductivity was 1–2 μS/cm. The plasma activation times 3, 4, and 5 min in a batch closed reactor gave PAW conductivities of 700 μS/cm, 975.5 μS/cm, and 1175 μS/cm, respectively, while the open TS-electrospray reactor made PAW of 474 ± 5 μS/cm. This variable PAW conductivity strongly influenced the amplitude and shape of the square high voltage pulses from the generator. To apply PEFs of similar current/voltage pulse characteristic for the experimental condition "PAW + PEF" and the condition "PEF only", the conductivity of the control was adjusted to 700 μS/cm by the addition of NaCl in DW.

2.5 Chemical Measurements of RONS in PAW

Long-lived RONS in the PAW are measured by UV/VIS absorption colorimetric methods (spectrophotometer Shimadzu UV-1900).

For hydrogen peroxide H_2O_2, the colorimetric method described in the study mentioned in reference [56] is applied. A volume of 100 μL of PAW sample is mixed with 10 μL of sodium azide to eliminate the nitrite which reacts with H_2O_2 and then 50 μL of titanium sulfonate reagent is added to produce pertitanic acid (**Eq.10**), a yellow color complex, with an absorption peak at 407 nm. According to Lambert–Beer's law, the concentration of hydrogen peroxide is proportional to the absorption (our calibration gives a molar extinction coefficient $\varepsilon = 4{,}03 \times 10^2\ \mathrm{L\,mol^{-1}.cm^{-1}}$).

$$Ti^{4+} + H_2O_2 + 2H_2O \rightarrow H_2TiO_4 + 4H^+ \qquad (10)$$

In the same way, nitrite NO_2^- concentration is measured using a Nitrate/Nitrite Colorimetric Assay Kit (# 780001, Cayman Chemicals) to proceed with the measurement of the absorption peak at 540 nm. However, the typical PAW nitrite concentration is too high for the measurement, thus 1:40 dilution of the PAW in DW is applied. We sampled 50 μL to mix with the 25 μL Griess reagent 1 and then 25 μL of Griess reagent 2 of the kit. After waiting 10 min for the coloration, the absorption peak was processed with the molar extinction coefficient $\varepsilon = 2.10 \times 10^2\ \mathrm{L\,mol^{-1}\,cm^{-1}}$.

The pH is a key parameter in the PAW chemistry and antibacterial effects [15]. It is measured just after PAW production, using the VTW PH 31–10 pH meter calibrated by 3-point method and after stabilization. The PAW conductivity is measured by using the GREISINGER electronic GMH 3430 conductivity meter.

3 RESULTS AND DISCUSSION

3.1 Transient Spark Discharge Characteristics

As shown in **Figure 3**, DC-driven TS-B and TS-ES discharges in positive polarity were generated in the point-to-plane configuration in ambient air at atmospheric pressure. The TS discharge pulse is always preceded by one or a sequence of small current (~10 mA) pulses, that is, streamers. For TS-ES (**Figure 3B**), a steep voltage drop of about 15–20 kV occurs during the strong current pulse of about 15–25 A, for a typical duration of about 20 ns. For TS-B (**Figure 3A**), the voltage drop is shallower and takes about 1 μs during a weaker current pulse of 2.5 A.

TS-ES electrical characteristic is quite stable in time, as this discharge occurs between two metal electrodes (needle-mesh). But for TS-B, in the beginning of the deionized water (DW) plasma exposition, the current pulse/voltage drop duration is very long (several μs). After a few seconds, the pulse duration becomes considerably shorter and reaches its typical μs drop time duration. Along with this pulse duration reduction of the discharge, the current pulse amplitude tends to increase from several hundred mA to several A. The PAW generated between the ground electrode and the positive needle electrode represents an RC circuit. Penetration of plasma charged particles (H^+, NO_2^-, and NO_3^-) progressively increased the conductivity of the treated water from 2 μS of DW to its final value and so decreased the resistivity of the liquid that could explain this temporal evolution of the electrical characteristic of TS-B (**Figure 3A**). The difference between the current pulse characteristics of TS-B and TS-ES may influence the produced RONS concentrations in PAW, although open air vs. closed reactor conditions influenced the RONS composition even more significantly. The typical power for the PAW generation is about 3W in both TS-ES and TS-B.

3.2 PEF Characteristics–U, I for Different Liquid Conductivities

Figure 4 shows the typical voltage and current pulse of the PEF treatment: a voltage of 2.5 kV amplitude, that is, the electric field of 12.5 kV/cm for the 2 mm spacing in the electroporation cuvette. Bacteria in the LBB culture medium used for the overnight culture were diluted 1:100 in different PAWs or in DW for the control condition. The conductivity of the control condition was adapted to 700 μS/cm with NaCl added to DW before adding bacteria, which is a typical conductivity of PAW (after 3 min TS-B treatment). The adaptation of the conductivity was necessary to obtain a similar I/U pulses for all PEF treatments, since the current pulse amplitude and shape strongly depend on the water conductivity. Application of PEF in the higher-conductive liquid also leads to its heating. The mean pulse power was 0.7 W dissipated in thermal energy into the cuvette.

3.3 PAW Chemistry–RONS

3.3.1 Open Air Transient Spark With Water Electrospray (TS-ES)

Figure 5A shows the time evolution of H_2O_2 and NO_2^- concentration in PAW prepared by TS-ES in open air. In this condition, 5 ml PAW was generated by 1 kHz transient spark discharge with a 1 ml/min deionized water (DW) flow rate and collected in a Petri dish to be analyzed. The concentration of H_2O_2 and NO_2^- in acidic PAW is known to decrease with time elapsed after the discharge is stopped [28]. In **Figure 5A**, t=0 is the moment when the discharge was turned off. The chemical measurement was performed independently of the bacteria

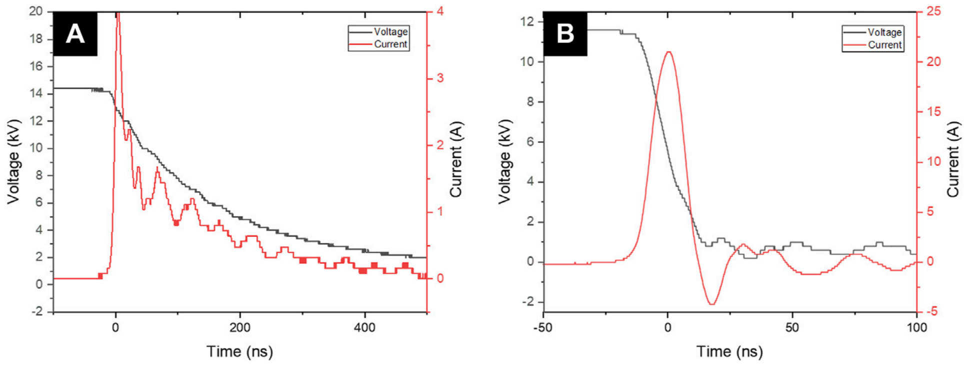

FIGURE 3 | Typical voltage/current waveforms for **(A)** TS-B for 3 min treatment at 1 kHz. **(B)** TS-ES at 1 kHz and 1 ml/min water flow rate.

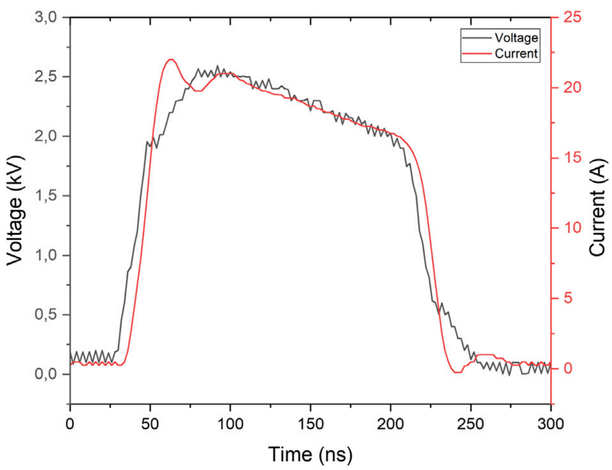

FIGURE 4 | Typical electrical characteristic of the PEF applied in the electroporation cuvette with PAW.

experiment for technical reasons (note that the incubation of bacteria in PAW started at t= 2 min 30 s). The measured PAW pH=3.5 ± 0.3 was stable with time t. In the first measurement (at t=1 min), H_2O_2 concentration was 430 µM and that of NO_2^- was 290 µM. These two reactive species both decayed with time. The concentration of H_2O_2 decayed rapidly to 380 µM until 3 min and then stabilized, reaching 350 µM after 17 min NO_2^- and decayed quasi-linearly from its initial concentration 290–110 µM at t=17 min. After the treatment the concentration of H_2O_2 dominated over the concentration of NO_2^- with a ratio H_2O_2/NO_2^- = 3/2. The significantly higher solubility of H_2O_2 transfers it into the PAW more vigorously than the other RONS. In the beginning of the water activation, NO_2^- and H_2O_2 are generated, and the reaction (**Eq. 8**) generating peroxynitrite depletes about the same molar parts of NO_2^- and H_2O_2 in the PAW. After the TS-ES plasma treatment, the minor NO_2^- is progressively consumed by the major H_2O_2 in this reaction, while the concentration of H_2O_2 then remains relatively stable. NO_2^- itself is also instable in acidic condition *via* the disproportionation reaction (**Eq. 14**) [57].

3.3.2 Closed Air Reactor Transient Spark Batch Treatment (TS-B)

In the closed reactor batch treatment (TS-B) (**Figure 5C**), the initial concentration of H_2O_2 in this PAW was lower (100 µM) than that in the open reactor, and the concentration of NO_2^- was higher (840 µM). With time after plasma activation, the H_2O_2 concentration fell to nearly zero (about 20 µM) after 5 min in an exponential trend decrease. The NO_2^- concentration also decreased exponentially; after 5 min it was 640 µM and after 17 min it was 500 µM. Gaseous concentrations of NO and NO_2 and HNO_2were much larger due to their longer accumulation in the reactor volume. The water vapors also accumulated reinforcing the RONS production. HNO_2 molecules, besides H_2O_2, are also readily dissolved in water, resulting in aqueous nitrites NO_2^- and acidification of the PAW [1, 30]. In these conditions, NO_2^- dominated over H_2O_2 at a ratio H_2O_2/NO_2^-= 1/6, and the same peroxynitrite reaction (**Eq. 8**) consumed all the remaining minor H_2O_2. plus NO_2^- also continuously dissociated to radicals (**Eq.12**) [9], or formed a nitrosonium ion *via* HNO_2 protonation reaction (**Eq.13**) [28]. NO_2^- was also disproportionated by the reaction in acidic conditions (**Eq. 14**), which is pH-dependent and occurs faster at pH < 3.5 [24, 57].

$$2HNO_2 \rightarrow {}^{\bullet}NO + {}^{\bullet}NO_2 + H_2O \quad (12)$$

$$HNO_2 + H^+ \rightarrow H_2NO_2^+ \rightarrow NO^+ + H_2O \quad (13)$$

$$3NO_2^- + 3H^+ \rightarrow 2{}^{\bullet}NO + NO_{3-} + H_3O^+ \quad (14)$$

3.3.3. Post-Discharge Time Evolution of RONS After Adding 1 mM H_2O_2 in PAW

Figures 5B,D show the time evolution of the concentration of hydrogen peroxide and nitrite in PAW TS-ES and TS-B, respectively, after adding 1 mM H_2O_2. Adding H_2O_2 after plasma treatment increased the measured concentration of H_2O_2. The concentration in NO_2^- dropped faster than in the condition without the addition of H_2O_2 due to its mutual reaction with H_2O_2 (**Eq. 8**).

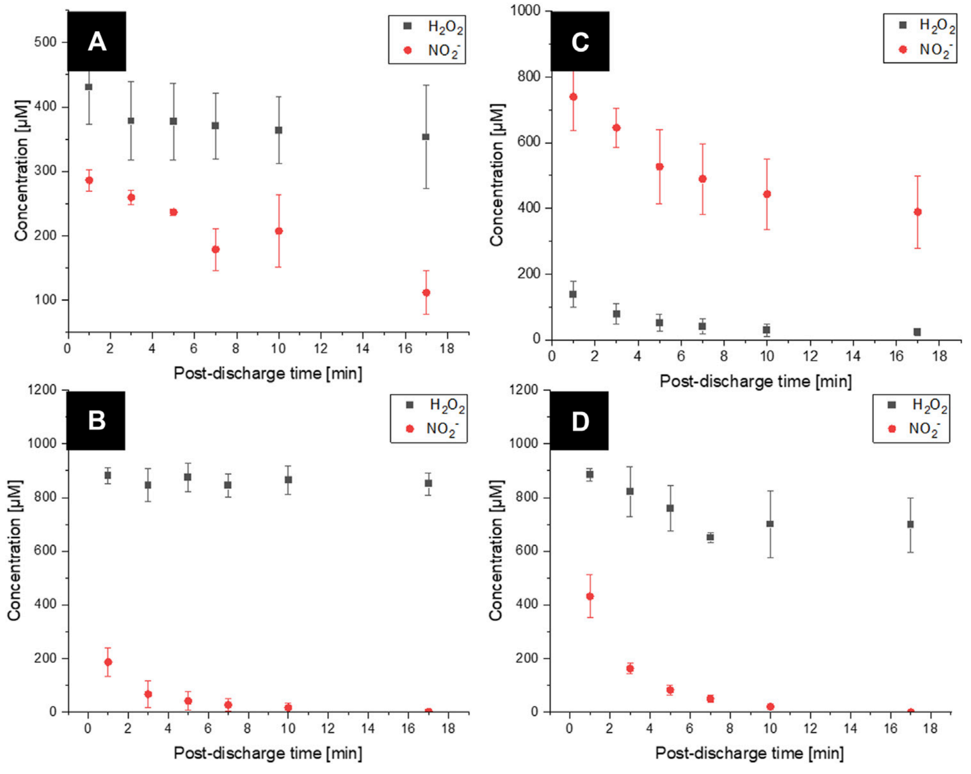

FIGURE 5 | Temporal evolution of H_2O_2 and NO_2^- concentrations in PAW prepared by **(A)** TS-ES (1 ml/min, 1 kHz) in open air. **(B)** TS-ES after adding 1 mM of H_2O_2. **(C)** TS-B (1 kHz, 5 min treatment) in the closed air reactor for 5 ml of DW. **(D)** TS-B after adding 1 mM of H_2O_2, closed air reactor for 5 ml of DW, 1 kHz.

In TS-B PAW after adding 1 mM H_2O_2 (**Figure 5D**), a higher initial concentration in H_2O_2 of 900 µM than in the standard TS-B closed air PAW and a lower NO_2^- concentration were measured at t = 1 min. The decay of both species was also faster. At 5 min, NO_2^- concentration was 100 µM and after 10 min it was close to zero. In the condition TS-B + H_2O_2, the concentration of NO_2^- and H_2O_2 stabilized faster than in the conditions without adding H_2O_2 in both closed (TS-B) and open air (TS-ES). When 1 mM H_2O_2 is added into PAW generated by TS-B closed and TS-ES open air (**Figures 5B,D**), the concentrations of H_2O_2 are stronger than in the original PAW TS-B and TS-ES without H_2O_2 addition, while the concentration of NO_2^- is supposed be the same (the decay of the first minute after PAW production changes the first measurement at 1 min). After H_2O_2 addition, we can expect an important enhancement of the ONOOH formation (**Eq. 8**) and its subsequent decay to radicals, which is proportional to the H_2O_2 concentration drop. In TS-B the first 5 min, the concentration of H_2O_2 dropped to 650 µM considering that the initial concentration of H_2O_2 in PAW was around 100 µM and the concentration of the added H_2O_2 was 1 mM. By approximate interpolation, a production of 450 µM of peroxynitrite would lead to the production of 135 µM of $^{\bullet}OH$ and $^{\bullet}NO_2$, assuming 30% conversion to these radicals. On the other hand, in TS-ES, the addition of 1 mM of H_2O_2 (**Figure 5B**) enhanced the concentration of already major H_2O_2, which resulted in a complete depletion of NO_2^- and accelerated the kinetic of the ONOOH reaction (**Eq. 8**), but in a less drastic way than in TS-BC.

3.4 Antibacterial Effects

3.4.1 PEF Only and H_2O_2 Only

The antibacterial effect can be expressed by two ways: 1) as a direct reduction of the bacteria population in CFU/ml with respect to the control condition, as shown in **Figures 6–8**; or 2) in log reduction (**eq. 15**) of the number of bacteria divided by the number of bacteria in the control condition, as shown in **Figure 9**.

$$Effect(Treatement) = -log_{10}[(Median(Treatement) \times / Median(Control)] \tag{15}$$

The PEF treatment of 12.5 kV/cm for a pulse duration of 200 ns at a frequency of 100 Hz during a treatment time of 100 s, applied to the *E. coli* showed no antibacterial effect (**Figure 6**). This PEF treatment was chosen to be mild to accentuate its synergic effect with PAW and not the antibacterial effect of the PEF itself. A PEF treatment with a longer duration of the pulse or a stronger electric field magnitude can result in a higher efficiency. Also, more repetitions of the pulses can lead to an antibacterial effect due to irreversible electroporation [58], but our mild PEF treatment did not show any lethal effect. The strong electric current circulating in the cuvette during the application

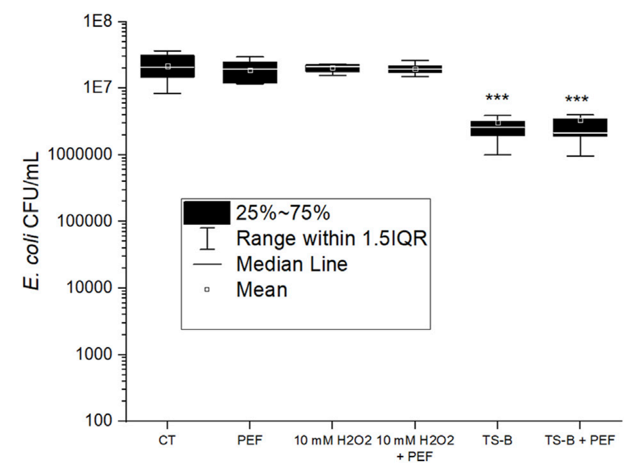

FIGURE 6 | *E. coli* population (CFU/ml) for PEF treatment only, 10 min incubation in 10 mM H_2O_2 only, and with PEF treatment, PAW generated by TS-B closed air reactor, 10 min incubation in PAW only and coupled with PEF treatment. One-way ANOVA test, (*) p-value < 0.05; (**) p-value < 0.01; and (***) p-value < 0.001 with respect to control (CT). Boxes and whiskers show the median, mean value, interquartile range (IQR), and error bars corresponding to 1.5IQR.

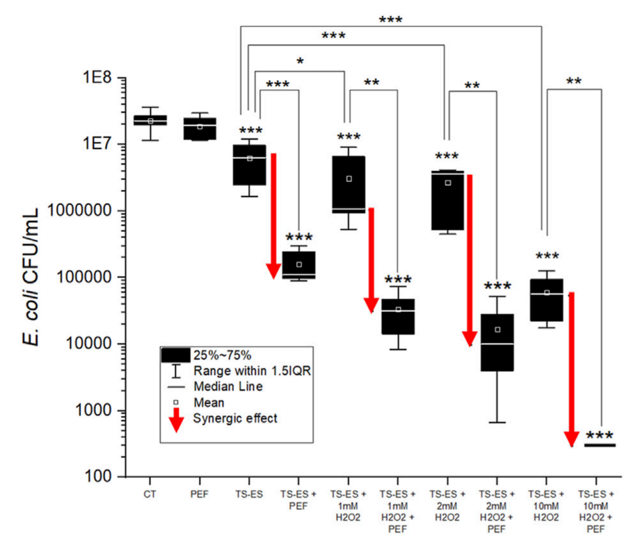

FIGURE 7 | *E. coli* population (CFU/ml) for the different treatments in PAW induced by TS-ES open air reactor without and with adding different concentrations of H_2O_2 and without and with PEF treatment. One-way ANOVA test, (*) p-value < 0.05; (**) p-value < 0.01; and (***) p-value < 0.001 with respect to control (CT), or other conditions as indicated by lines. Boxes and whiskers show the median, mean value, interquartile range (IQR), and error bars corresponding to 1.5IQR. Red arrows indicate the bacterial population reduction due to synergy of PEF and PAW.

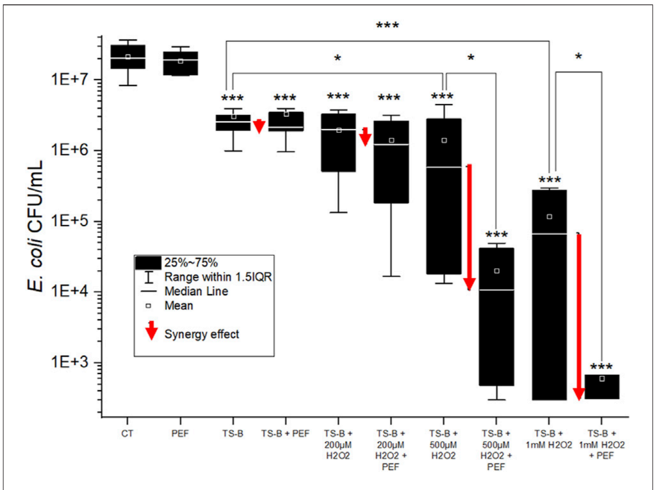

FIGURE 8 | *E. coli* population (CFU/ml) for the different treatments in PAW induced by the TS-B closed air reactor without and with adding different concentrations of H_2O_2 and without and with PEF treatment. The white dot is the mean, black line in the gray scar is the median, square is the Q1 and Q3, and the whiskers are the extremes value of the experiment. One-way ANOVA test, (*) p-value < 0.05; (**) p-value < 0.01; (***) p-value < 0.001 with respect to control (CT), or other conditions as indicated by lines. Boxes and whiskers show the median, mean value, interquartile range (IQR), and error bars corresponding to 1.5IQR. Red arrows indicate the bacterial population reduction due to synergy of PEF and PAW.

produced a temperature increase of a few degrees (from 21 to 30–34°C measured by a thermocouple) for a power of the PEF of approximately 0.7 W. This increase in temperature is known to speed up the pore formation [59, 60]. To prevent this phenomenon from causing a difference in behavior between the control condition and the PAW, the conductivity of the control condition and H_2O_2 only conditions was adapted to 700 µS/cm (like PAW), as mentioned previously in **Section 2.4** and **Section 3.2**. The same conductivity is needed to obtain the same current/voltage pulse in the cuvette for PAW and for the control or H_2O_2-only conditions.

In the objective to investigate the antibacterial effect of H_2O_2 only and its potential interactions with PEF treatment, we tested the highest concentration, 10 mM, which was added in DW, incubated with *E. coli* and applied PEF treatment during the incubation. The concentration of H_2O_2 which was added into the PAW was tested in the range 100 µM–10 mM. It is well known that H_2O_2 as a medical disinfectant is used in much higher concentrations (3% vol., i.e., 0.98 M). H_2O_2 is also often considered as the key antibacterial or antitumor agent of PAW in synergy with other RONS [61]. However, in our studied maximum concentration of 10 mM H_2O_2 diluted in DW, we did not observe any antibacterial effect (**Figure 6**) by H_2O_2 itself, nor H_2O_2 combined with PEF. In the PAW studied here, plasma-generated H_2O_2 concentration did not exceed 600 µM in TS-ES open air discharge and 150 µM in TS-B closed reactor. Even with the addition of 100 µM–1 mM H_2O_2 in the TS-B or 1–10 mM H_2O_2 in TS-ES, we operated in the range of H_2O_2 concentrations far below those where it is typically used as a disinfectant.

Considering this, H_2O_2 alone should not be considered as the key antibacterial plasma agent. We can hypothesize that H_2O_2 only cannot be responsible for an efficiency of PEF treatment by penetration through the membrane into the cell or by facilitation of pore formation by peroxidation of the membrane. However, its interaction with other species in the PAW, especially nitrites, makes it a key species resulting in the PAW antibacterial effect, which was even enhanced by PEF, as discussed later.

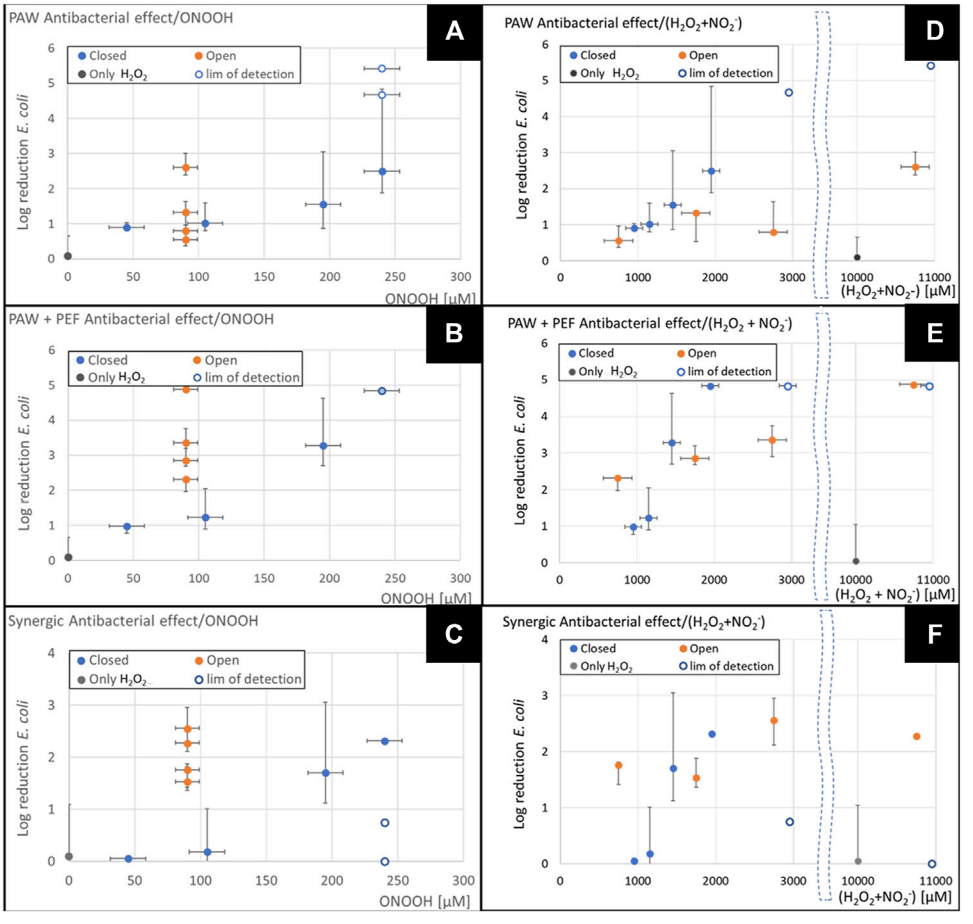

FIGURE 9 | Antibacterial effects expressed as log reduction as a function of the sum of NO_2^- and H_2O_2 **(A–C)** and estimated ONOOH concentration **(D–F)**. **(A,D)** PAW antibacterial effect. **(B,E)** Total antibacterial effect of PAW with PEF. **(C,F)** Synergic antibacterial effect expressed as the difference between the total antibacterial effect and the PAW only antibacterial effect.

3.4.2 Open Air TS-ES PAW + PEF

To investigate a coupled antibacterial effect on *E. coli* of the plasma agents in PAW with PEF treatment, we first incubated the bacteria in PAW generated by the open-air TS-ES discharge. As shown in **Figure 7**, the 10 min incubation in this PAW obtained a significant antibacterial effect of 0.8 log. The applied PEF treatment during the incubation resulted in the log reduction of 2.2 which represents a synergic effect of 1.4 log. Adding 1, 2 and 10 mM of H_2O_2 in the PAW further increased the antibacterial effect. The effect of PEF treatment of these PAW + H_2O_2 conditions also strongly increased the synergy PAW + PEF effect. The log reduction value for the highest added H_2O_2 concentration (10 mM), is near the detection limit of our microbial cultivation method considering the dilutions (leading to complete sterilization).

Considering our PEF only treatment antibacterial effect is nearly zero, the synergy effect was defined by **Eq.16** as a difference between the total PAW + PEF antibacterial effect and the effect of PAW only (in $\log_{10}$ reduction) [62]

$$\text{Synergy}\,(\text{PAW}, \text{PEF}) = \text{Log}_{10}\,(\text{PAW} + \text{PEF}) - \log_{10}\,(\text{PAW}) \tag{16}$$

In the PAW produced in open-air TS-ES condition (**Figure 7**), we obtained the antibacterial effect stronger with the addition of PEF than by incubation in PAW only. This synergic antibacterial effect further increased with adding increasing concentrations of H_2O_2 into the PAW. Increasing H_2O_2 concentration in this H_2O_2-dominated PAW did not increase the final product of peroxynitrite (**eq. 8**) but increased the kinetic of its production and thus increased the quantity of ONOOH and its decay products (radicals OH and NO_2) in contact with bacteria. Additional PEF probably facilitated their penetration through the cell membrane and resulted in the stronger antibacterial effect.

3.4.3 Closed Air TS-B PAW + PEF

The antibacterial effect of TS-B PAW prepared in the closed air reactor and measured without and with the PEF t and with additions of H_2O_2 (from 0.2 to 10 mM concentration), is shown in **Figure 8**. PAW only antibacterial effect, as well as PAW + PEF were about 1 log. Adding hydrogen peroxide to the PAW, especially 500 µM and 1 mM, significantly increased its

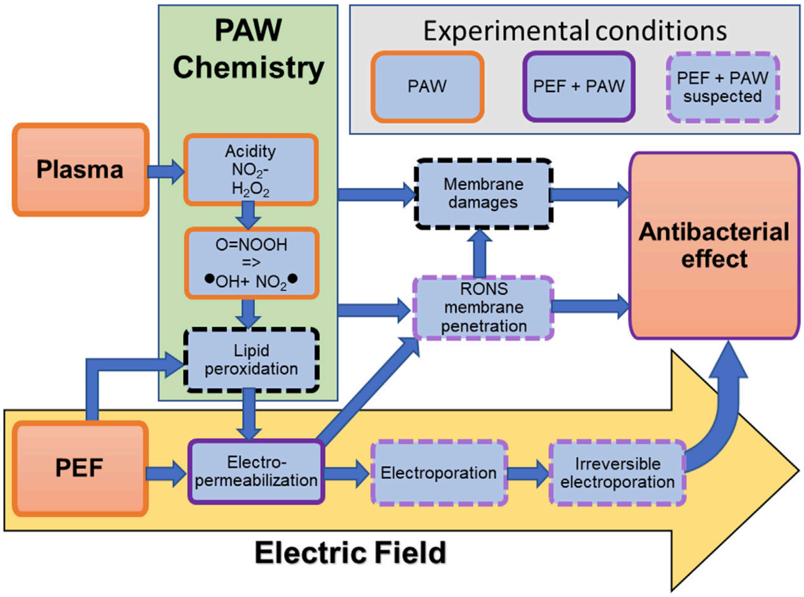

FIGURE 10 | Summarizing schematics of the interaction between NO_2^- and H_2O_2 and bacterial incubation in PAW reinforced by the PEF treatment.

antibacterial effect. PAW + H_2O_2 combined with PEF treatment induced a strong synergic antibacterial effect.

The antibacterial effects of the PAW open air TS-ES and PAW closed air TS-B are similar, but coupled with PEF treatment, the open-air TS-ES PAW showed a synergy effect, unlike the closed reactor TS-B PAW, which showed no synergy effect with the same PEF treatment. However, adding H_2O_2 of concentrations 100 μM, 200 μM, 1 mM, 2 and 10 mM to the TS-B PAW have shown a strong and increasing antibacterial effect. The complete sterilization was often observed for the added H_2O_2 concentrations of 1 and 2 mM, and always for 10 mM. In these cases, the minimum number of colonies was fixed at 300 that corresponds to one colony for every measurement of each experiment repetition. This represents the limit of detection of the countable CFUs. The PEF treatment of these PAW + H_2O_2 conditions increased the antibacterial effect by increasing the synergic PAW + PEF effect, although less intensely than for TS-ES PAW.

It is interesting that the antibacterial effect of TS-B PAW in the closed air reactor (**Figure 8**) was as intense as that of TS-ES PAW in the open-air (**Figure 7**), although PAW in the closed and open air had a different RONS composition. In addition to the reaction between H_2O_2 and NO_2^- (**Eq. 8**) producing ONOOH and radicals, the high NO_2^- concentration could enhance the antibacterial effect due to the nitrite/nitrous acid NO_2^-/HNO_2 (pKa=3.4). This acidic form of HNO_2 (also called acidified nitrite) is also strongly antibacterial [24,63]. The formation of nitrogen radicals $^{\bullet}NO$ and $^{\bullet}NO_2$ by **Eq. 12** is more likely the main reason of the induced antibacterial effect that substantially inhibited the growth of *E. coli* under acidic conditions. It should be stressed out that in the closed air TS-B PAW, the additional PEF treatment during showed no extra antibacterial effect (unless H_2O_2 was added). It seems that electro-permeabilization by the PEF treatment combined with NO_2^--rich PAW does not lead to the synergic effect in this condition.

On the other hand, when adding H_2O_2, the antibacterial effect increased much more in TS-B than in TS-ES open air for the same added H_2O_2 concentrations. As discussed earlier in the chemical part, the dynamic of the reaction between H_2O_2 and NO_2^-, the production of peroxynitrite depends on the concentration of the dominant species. Thus, adding H_2O_2 to the TS-B PAW normally dominated by NO_2^- increased much more the production of ONOOH than in the open-air TS-ES PAW. The production of radicals as decay products of ONOOH also increased and so PEF facilitated their penetration into the cells, which is correlated with the increase of the antibacterial effect.

Radicals in contact with the cell membrane cause lipid peroxidation that facilitate the electropermeabilization of the membrane by the PEF treatment. The present data cannot conclude if the synergic antibacterial effect is due to the fragilization of the membrane leading to irreversible electroporation during the PEF treatment or an improvement of RONS lethal activity by passing through the cell membrane and attacking bacterial organelles, DNA, and the internal layer of bacteria membrane's phospholipids.

3.4.4 Quantification of the Antibacterial Effects in Function of the RONS Concentration

The experiments were performed to investigate the correlations and synergies between the RONS in the PAW and their antibacterial effects tested on *E. coli* incubated in PAW only, PAW enriched with hydrogen peroxide, and in PAW and PAW + H_2O_2 coupled with the PEF treatment.

Figures 9A–C shows on the x-axis the sum of the measured concentrations of the key RONS: NO_2^- + H_2O_2. The x-error bar is the Euclidean distance or 2-norm (**eq.17**) of the standard deviations of both these components from their initial measurements without adding H_2O_2, as shown in **Figures 5–A,C**.

$$X_{error} = \sqrt{\left(Stdev_{H_2O_2}\right)^2 + \left(Stdev_{NO_2^-}\right)^2}, \tag{17}$$

$$Error\,(\mathrm{Q1}\ or\ \mathrm{Q3}) = log_{10}\left(\frac{Control}{\mathrm{Q1}\ or\ \mathrm{Q3}_{treatment}}\right) - log_{10}\left(\frac{Control}{Median_{treatment}}\right) = log_{10}\left(\frac{Median_{treatment}}{\mathrm{Q1}\ or\ \mathrm{Q3}_{treatment}}\right) \tag{18}$$

The log reduction of *E. coli* in **Figure 9** is shown as the log10 of the median value of each condition divided by the median value of the control (**Eq. 15**), the same medians shown in **Figures 6–8**. The asymmetric error bars are calculated by **Eq. 18** where Q1 and Q3 are the first and third quartiles of the *E. coli* population in each treatment condition (as shown in the box graph in **Figures 6–8**). In the cases of the complete sterilization, we have taken the number of 300 CFU/mL as the detection limit, which corresponds to one colony grown in the lowest dilution on the Petri dish. This minimum CFU/mL value impacts the error bar for the strongest antibacterial treatments (TS-B closed reactor with added 1 mM of H_2O_2 with and without PEF, TS-B closed with added 500 μM of H_2O_2; and open-air TS-ES with added 10 mM of H_2O_2).

Figures 9A–C show that the antibacterial effect increased with the total RONS concentration in a stronger way for the closed TS-B condition than for the TS-ES open condition. The increase of the total RONS is directly linked with the addition of H_2O_2, which for the open TS-ES reactor simply increased its concentration in the PAW, while for the closed TS-B reactor this also increased the ONOOH concentration, hence the NO_2^-/H_2O_2 degradation kinetics leading to radicals $^\bullet$OH and $^\bullet NO_2$. This impact on the kinetic cannot be represented in this figure but it must be considered to understand which RONS interact with the cell membrane during the PEF treatment. **Figure 9A** suggests a stronger antibacterial effect of the PAW which forms these radicals produced by the degradation of ONOOH. In the **Figure 9C** the synergic effect increased drastically in the PAW TS-B with the increased total RONS, that is, with the addition of $H_2O_{2,}$ thus enhancing ONOOH, while the increase of the total RONS in TS-ES affected the synergic effect much less. Hydrogen peroxide therefore has a much weaker synergic effect than ONOOH and only in the presence of the latter. However, H_2O_2 should be considered in the antibacterial effect of PAW alone and in the synergy antibacterial effect of PAW and PEF especially in presence of radical $^\bullet$OH and $^\bullet NO_2$ in the PAW.

The estimated ONOOH concentration from the **Eq. 8** in **Figures 9D–F**, shown in the x-axis is obtained from the minimum mean concentration of either H_2O_2 or NO_2^- (the lower one) for each condition. Peroxynitrous acid (ONOOH) is on 70% turned into NO_3- and H^+, with the pH is unchanged because the reaction of H_2O_2 with NO_2^- needs H^+ ions to occur. The other 30% of ONOOH creates $^\bullet$OH and $^\bullet NO_2$ radicals which are known for their strong antibacterial effect and lipid peroxidation. The concentration of H_2O_2 taken for the estimation of ONOOH concentration is the measured H_2O_2 after plasma activation, plus the pre-set concentration of the externally added H_2O_2. The x-error bars in **Figures 9D–F** are the standard deviations of the initial H_2O_2 or NO_2^- values measured from three repetitions, corresponding to the y-error bars shown in **Figure 5** at t= 1 min.

In **Figure 9D**, TS-ES open air shows a constant concentration of ONOOH estimated to 300 μM for all the conditions because the less concentrated species from either H_2O_2 or NO_2^- is the NO_2^-. Its initial concentration was not affected by the addition of hydrogen peroxide, so the ONOOH concentration remained presumably constant, based on the ONOOH formation by **Eq. 8**. On the other hand, in the condition TS-B closed air reactor shown in **Figure 9D**, the log reduction values increase with the ONOOH concentrations until 800 μM, because the dominant species is the nitrite, and the limiting species is H_2O_2. Above 800 μM ONOOH (i.e., in cases of the added 1 mM H_2O_2 or more), the concentration of ONOOH becomes limited by nitrite at 800 μM, similar to the limit of 300 μM in the TS-ES open case. We excluded the condition TS-B closed reactor with the addition of 2 and 10 mM H_2O_2 in **Figure 9** because the antibacterial effect of the PAW only is already the complete sterilization and so cannot bring any information on the synergy effect of the nitrite and hydrogen peroxide with PEF treatment.

Figures 9D–F from TS-B closed reactor shows that the increase of ONOOH enhanced the antibacterial effect and also the synergic effect with PEF. We observed that the antibacterial effect of the TS-ES open air PAW was lower than that of the TS-B closed for the same concentration of ONOOH, but the synergic effect (**Figure 9F**) for the TS-ES was stronger than in the TS-B for the same concentration of ONOOH. The antibacterial effect of H_2O_2 and the synergic effect of H_2O_2 with PEF was zero. This result suggests that the presence of ONOOH in the PAW reinforces the effect of the hydrogen peroxide itself and give it a synergic effect with PEF. It was shown by [64] that H_2O_2 was synergized with longer pulses duration. Maybe the effect of the radicals produced from the ONOOH caused a sublethal damage of the cell membrane facilitating the peroxidation of the phospholipids by the H_2O_2, which alone had no antibacterial effect, nor was synergic with PEF.

4 CONCLUSION

The antibacterial effects of atmospheric cold plasma and plasma-activated water are usually investigated separately of the bactericidal treatments of the pulsed electric fields, despite common physicochemical mechanisms and industrial applications. The cold plasma is generated by applying an electric field, hence could lead to electropermeabilization/electroporation mechanisms that contribute in part to the antibacterial effect. PEF treatments generate intracellular RONS and cause lipid peroxidation, and RONS production by PEF treatment is a key factor of the initiation of pore formation in the cell membrane, a promoting factor for a pore growth and for a decrease of the minimum voltage for triggering electroporation.

We investigated the antibacterial effect of PEF and PAW treatment of *E. coli* individually and in synergy. Chemical measurement of nitrite and H_2O_2 and antibacterial effects were tested for two types of PAW, generated by transient spark discharge with electrospray in open air (TS-ES) and the same discharge in batch treatment in closed reactor with air (TS-B). This enabled us to obtain different PAW chemistry processes and different roles of the PAW components acting in synergy with PEF in the antibacterial effect. In addition, the PAW was externally doped by the addition of H_2O_2, and its effect on bacteria coupled with PEF was tested.

PAW generated by TS-ES in open air achieved a ratio of dominant RONS: $H_2O_2/NO_2^- = 3/2$, whereas TS-B PAW in closed reactor reached the ratio $H_2O_2/NO_2^- = 1/6$ due to the accumulation of gaseous NOx in air which are absorbed in the water to form nitrites and protons (H^+). Hydrogen peroxide is extremely soluble and is absorbed more easily by the liquid. Once NO_2^- and H_2O_2 are in the PAW under acidic pH, they react into peroxynitrous acid ONOOH, an instable RONS which further decays into $^{\bullet}OH$ and $^{\bullet}NO_2$ radicals.

Despite different RONS in the TS-ES and the TS-B PAW, their antibacterial effects were comparable. In the closed reactor (TS-B) the lower pH and higher concentration of NO_2^- could be a major factor, while in open reactor (TS-ES) the antibacterial effect could be mainly due to the presence of similar concentrations of H_2O_2 and NO_2^- which react in acidic conditions to form ONOOH, which then decays in radicals. Adding H_2O_2 to NO_2^--rich TS-B closed reactor PAW resulted in a stronger boost of the antibacterial effect than in TS-ES open reactor PAW with similar concentrations of H_2O_2 and NO_2^-. The synergic effect of PEF with PAW was observed only if enough NO_2^- and H_2O_2 were present and was reinforced with their increase. This suggests than peroxynitrous acid and radicals, such as $^{\bullet}OH$, are key species in antibacterial effect of PAW but also a major factor in the investigated synergy treatments by coupled PAW + PEF.

Figure 10 schematically summarizes the RONS (in the PAW) synergic antibacterial effects with PEF. Knowing if these PEF + PAW combined treatments lead to permeabilization of the cell membrane which would enhance the effect of RONS, or whether the weakening of the membrane will lead to irreversible electroporation, remains an open question. Repeating these experiments with bacteria of different types, in different states, such as biofilms or spores, is necessary in future to make the method generally usable. The understanding of plasma–pulsed electric field–RONS interactions is important not only in bacterial decontamination, but its results can be exploited in other applications, such as wound healing, cancer therapy, food industry, and agriculture.

DATA AVAILABILITY STATEMENT

The raw data supporting the conclusions of this article will be made available by the authors, without undue reservation.

AUTHOR CONTRIBUTIONS

RM ran and processed the experiments and wrote the first draft manuscript. ZM planned, organized, and supervised the research, and reviewed and edited the manuscript. All authors have read and agreed to the published version of the manuscript.

FUNDING

This study was supported by the grant of the Slovak Research and Development Agency (APVV-17-0382) and Slovak Grant Agency VEGA (1/0596/22).

ACKNOWLEDGMENTS

The authors thank Barbora Tarabova (IPP, ASCR Prague) for the help with initial experiments.

REFERENCES

1. Jablonowski H, von Woedtke T. Research on Plasma Medicine-Relevant Plasma-Liquid Interaction: What Happened in the Past Five Years? *Clin Plasma Med* (2015) 3(2):42–52. doi:10.1016/j.cpme.2015.11.003
2. Fridman A, Friedman G. *Plasma Medicine*. John Wiley & Sons (2012). p. 293–338.
3. Chen C, Smye SW, Robinson MP, Evans JA. Membrane Electroporation Theories: A Review. *Med Bio Eng Comput* (2006) 44(1–2):5–14. doi:10.1007/s11517-005-0020-2
4. Kotnik T, Rems L, Tarek M, Miklavčič D. Membrane Electroporation and Electropermeabilization: Mechanisms and Models. *Annu Rev Biophys* (2019) 48:63–91. doi:10.1146/annurev-biophys-052118-115451
5. Casciola M, Tarek M. A Molecular Insight into the Electro-Transfer of Small Molecules through Electropores Driven by Electric fields. *Biochim Biophys Acta (Bba) - Biomembranes* (2016) 1858(10):2278–89. doi:10.1016/j.bbamem.2016.03.022
6. Nuccitelli R, Lui K, Kreis M, Athos B, Nuccitelli P. Nanosecond Pulsed Electric Field Stimulation of Reactive Oxygen Species in Human Pancreatic Cancer Cells Is Ca2+-dependent. *Biochem Biophysical Res Commun* (2013) 435:580–5. doi:10.1016/j.bbrc.2013.05.014
7. Szili EJ, Oh J-S, Fukuhara H, Bhatia R, Gaur N, Nguyen CK, et al. Modelling the Helium Plasma Jet Delivery of Reactive Species into a 3D Cancer Tumour. *Plasma Sourc Sci. Technol.* (2018) 27(1):014001. doi:10.1088/1361-6595/aa9b3b
8. Brisset J-L, Pawlat J. Chemical Effects of Air Plasma Species on Aqueous Solutes in Direct and Delayed Exposure Modes: Discharge, Post-Discharge and Plasma Activated Water. *Plasma Chem Plasma Process* (2016) 36(2):355–81. doi:10.1007/s11090-015-9653-6
9. Bruggeman PJ, Kushner MJ, Locke BR, Gardeniers JGE, Graham WG, Graves DB, et al. Plasma-Liquid Interactions: A Review and Roadmap. *Plasma Sourc Sci. Technol.* (2016) 25(5):053002. doi:10.1088/0963-0252/25/5/053002
10. Machala Z, Tarabova B, Hensel K, Spetlikova E, Sikurova L, Lukes P. Formation of ROS and RNS in Water Electro-Sprayed through Transient Spark Discharge in Air and Their Bactericidal Effects. *Plasma Process Polym* (2013) 10(7):649–59. doi:10.1002/ppap.201200113
11. Tarabová B, Lukeš P, Janda M, Hensel K, Šikurová L, Machala Z. Specificity of Detection Methods of Nitrites and Ozone in Aqueous Solutions Activated by Air Plasma. *Plasma Process Polym* (2018) 15(6):1800030. doi:10.1002/ppap.201800030
12. Chauvin J, Gibot L, Griseti E, Golzio M, Rols M-P, Merbahi N, et al. Elucidation of *In Vitro* Cellular Steps Induced by Antitumor Treatment with Plasma-Activated Medium. *Sci Rep* (2019) 9(1):1–11. doi:10.1038/s41598-019-41408-6

13. Liou G-Y, Storz P. Reactive Oxygen Species in Cancer. *Free Radic Res* (2010) 44(5):479–96. doi:10.3109/10715761003667554
14. Yan D, Malyavko A, Wang Q, Lin L, Sherman JH, Keidar M. Cold Atmospheric Plasma Cancer Treatment, a Critical Review. *Appl Sci* (2021) 11(16):7757. doi:10.3390/app11167757
15. Xu D, Wang B, Xu Y, Chen Z, Cui Q, Yang Y, et al. Intracellular ROS Mediates Gas Plasma-Facilitated Cellular Transfection in 2D and 3D Cultures. *Sci Rep* (2016) 6:27872. doi:10.1038/srep27872
16. Ndiffo Yemeli GB, Švubová R, Kostolani D, Kyzek S, Machala Z. The Effect of Water Activated by Nonthermal Air Plasma on the Growth of Farm Plants: Case of maize and Barley. *Plasma Process Polym* (2021) 18(1):2000205. doi:10.1002/ppap.202000205
17. Ozen E, Singh RK. Atmospheric Cold Plasma Treatment of Fruit Juices: A Review. *Trends Food Sci Technology* (2020) 103:144–51. doi:10.1016/j.tifs.2020.07.020
18. Haertel B, Woedtke Tv., Weltmann K-D, Lindequist U. Non-Thermal Atmospheric-Pressure Plasma Possible Application in Wound Healing. *Biomolecules Ther* (2014) 22(6):477–90. doi:10.4062/biomolther.2014.105
19. Bekeschus S, Schmidt A, Weltmann K-D, von Woedtke T. The Plasma Jet kINPen - A Powerful Tool for Wound Healing. *Clin Plasma Med* (2016) 4(1):19–28. doi:10.1016/j.cpme.2016.01.001
20. Gorbanev Y, O'Connell D, Chechik V. Non-Thermal Plasma in Contact with Water: The Origin of Species. *Chem Eur J* (2016) 22(10):3496–505. doi:10.1002/chem.201503771
21. Machala Z, Chládeková L, Pelach M. Plasma Agents in Bio-Decontamination by Dc Discharges in Atmospheric Air. *J Phys D: Appl Phys* (2010) 43:222001. doi:10.1088/0022-3727/43/22/222001
22. Pavlovich MJ, Sakiyama Y, Clark DS, Graves DB. Antimicrobial Synergy Between Ambient-Gas Plasma and UVA Treatment of Aqueous Solution. *Plasma Process Polym* (2013) 10:1051–60. doi:10.1002/ppap.201300065
23. Kurake N, Tanaka H, Ishikawa K, Takeda K, Hashizume H, Nakamura K, et al. Effects of OH and NO Radicals in the Aqueous Phase on H_2O_2 and NO2-Generated in Plasma-Activated Medium. *J Phys D: Appl Phys* (2017) 50(15):155202. doi:10.1088/1361-6463/aa5f1d
24. Machala Z, Tarabova B, Sersenova J, Hensel K. Chemical and Antibacterial Effects of Plasma Activated Water: Correlation with Gaseous and Aqueous Reactive Oxygen and Nitrogen Species. *J Phys D: Appl Phys* (2019) 52:03400217. doi:10.1088/1361-6463/aae807
25. Pavlovich MJ, Clark DS, Graves DB. Quantification of Air Plasma Chemistry for Surface Disinfection. *Plasma Sourc Sci. Technol.* (2014) 23(6):065036. doi:10.1088/0963-0252/23/6/065036
26. Jablonowski H, Bussiahn R, Hammer MU, Weltmann K-D, von Woedtke T, Reuter S. Impact of Plasma Jet Vacuum Ultraviolet Radiation on Reactive Oxygen Species Generation in Bio-Relevant Liquids. *Phys Plasmas* (2015) 22:122008. doi:10.1063/1.4934989
27. Locke BR, Shih K-Y. Review of the Methods to Form Hydrogen Peroxide in Electrical Discharge Plasma with Liquid Water. *Plasma Sourc Sci. Technol.* (2011) 20:034006. doi:10.1088/0963-0252/20/3/034006
28. Lukes P, Dolezalova E, Sisrova I, Clupek M. Aqueous-phase Chemistry and Bactericidal Effects from an Air Discharge Plasma in Contact with Water: Evidence for the Formation of Peroxynitrite through a Pseudo-second-order post-discharge Reaction of H2O2and HNO2. *Plasma Sourc Sci. Technol.* (2014) 23(1):015019. doi:10.1088/0963-0252/23/1/015019
29. Girard F, Badets V, Blanc S, Gazeli K, Marlin L, Authier L, et al. Formation of Reactive Nitrogen Species Including Peroxynitrite in Physiological Buffer Exposed to Cold Atmospheric Plasma. *RSC Adv* (2016) 6(82):78457–67. doi:10.1039/c6ra12791f
30. Janda M, Hensel K, Tóth P, Hassan ME, Machala Z. The Role of HNO2 in the Generation of Plasma-Activated Water by Air Transient Spark Discharge. *Appl Sci* (2021) 11:7053. doi:10.3390/app11157053
31. Laurita R, Barbieri D, Gherardi M, Colombo V, Lukes P. Chemical Analysis of Reactive Species and Antimicrobial Activity of Water Treated by Nanosecond Pulsed DBD Air Plasma. *Clin Plasma Med* (2015) 3(2):53–61. doi:10.1016/j.cpme.2015.10.001
32. Kruszelnicki J, Lietz AM, Kushner MJ. Atmospheric Pressure Plasma Activation of Water Droplets. *J Phys D: Appl Phys* (2019) 52:355207. doi:10.1088/1361-6463/ab25dc
33. Hassan M, Janda M, Machala Z. Transport of Gaseous Hydrogen Peroxide and Ozone into Bulk Water vs. Electrosprayed Aerosol. *Water* (2021) 13(2):182. doi:10.3390/w13020182
34. Wu S, Zhang Q, Ma R, Yu S, Wang K, Zhang J, et al. Reactive Radical-Driven Bacterial Inactivation by Hydrogen-Peroxide-Enhanced Plasma-Activated-Water. *Eur Phys J Spec Top* (2017) 226:2887–99. doi:10.1140/epjst/e2016-60330-y
35. Darny T, Pouvesle J-M, Puech V, Douat C, Dozias S, Robert E. Analysis of Conductive Target Influence in Plasma Jet Experiments through Helium Metastable and Electric Field Measurements. *Plasma Sourc Sci. Technol.* (2017) 26:045008. doi:10.1088/1361-6595/aa5b15
36. Lin L, Yan D, Gjika E, Sherman JH, Keidar M. Atmospheric Plasma Meets Cell: Plasma Tailoring by Living Cells. *ACS Appl Mater Inter* (2019) 11(34):30621–30. doi:10.1021/acsami.9b10620
37. Dozias S, Pouvesle JM, Robert E. Comment on 'Mapping the Electric Field Vector of Guided Ionization Waves at Atmospheric Pressure', (2020) Plasma Res. Express 2 025014. *Plasma Res Express* (2021) 3:038001. doi:10.1088/2516-1067/ac18b9
38. Rems L, Miklavčič D. Tutorial: Electroporation of Cells in Complex Materials and Tissue. *J Appl Phys* (2016) 119:201101. doi:10.1063/1.4949264
39. Tero R, Suda Y, Kato R, Tanoue H, Takikawa H. Plasma Irradiation of Artificial Cell Membrane System at Solid-Liquid Interface. *Appl Phys Express* (2014) 7(7):077001–6. doi:10.7567/APEX.7.077001
40. Yusupov M, Van der Paal J, Neyts EC, Bogaerts A. Synergistic Effect of Electric Field and Lipid Oxidation on the Permeability of Cell Membranes. *Biochim Biophys Acta (Bba) - Gen Subjects* (2017) 1861(4):839–47. doi:10.1016/j.bbagen.2017.01.030
41. Maccarrone M, Bladergroen MR, Rosato N, Agro AF. Role of Lipid Peroxidation in Electroporation-Induced Cell Permeability. *Biochem Biophysical Res Commun* (1995) 209:417–25. doi:10.1006/bbrc.1995.1519
42. Leduc M, Guay D, Leask RL, Coulombe S. Cell Permeabilization Using a Non-Thermal Plasma. *New J Phys* (2009) 11:115021. doi:10.1088/1367-2630/11/11/115021
43. Tero R, Yamashita R, Hashizume H, Suda Y, Takikawa H, Hori M, et al. Nanopore Formation Process in Artificial Cell Membrane Induced by Plasma-Generated Reactive Oxygen Species. *Arch Biochem Biophys* (2016) 605:26–33. doi:10.1016/j.abb.2016.05.014
44. Vernier PT, Levine ZA, Wu Y-H, Joubert V, Ziegler MJ, Mir LM, et al. Electroporating fields Target Oxidatively Damaged Areas in the Cell Membrane. *Plos One* (2009) 4:e7966. doi:10.1371/journal.pone.0007966
45. Zhang Q, Zhuang J, von Woedtke T, Kolb JF, Zhang J, Fang J, et al. Synergistic Antibacterial Effects of Treatments with Low Temperature Plasma Jet and Pulsed Electric fields. *Appl Phys Lett* (2014) 105:104103. doi:10.1063/1.4895731
46. Steuer A, Wolff CM, von Woedtke T, Weltmann K-D, Kolb JF. Cell Stimulation versus Cell Death Induced by Sequential Treatments with Pulsed Electric fields and Cold Atmospheric Pressure Plasma. *Plos One* (2018) 13(10):e0204916. doi:10.1371/journal.pone.0204916
47. Wolff CM, Steuer A, Stoffels I, von Woedtke T, Weltmann K-D, Bekeschus S, et al. Combination of Cold Plasma and Pulsed Electric fields - A Rationale for Cancer Patients in Palliative Care. *Clin Plasma Med* (2019) 16:100096. doi:10.1016/j.cpme.2020.100096
48. Wolff CM, Kolb JF, Weltmann K-D, von Woedtke T, Bekeschus S. Combination Treatment with Cold Physical Plasma and Pulsed Electric Fields Augments ROS Production and Cytotoxicity in Lymphoma. *Cancers* (2020) 12(4):845. doi:10.3390/cancers12040845
49. Banaschik R, Burchhardt G, Zocher K, Hammerschmidt S, Kolb JF, Weltmann K-D. Comparison of Pulsed corona Plasma and Pulsed Electric fields for the Decontamination of Water Containing *Legionella pneumophila* as Model Organism. *Bioelectrochemistry* (2016) 112:83–90. doi:10.1016/j.bioelechem.2016.05.006
50. Griseti E, Kolosnjaj-Tabi J, Gibot L, Fourquaux I, Rols M-P, Yousfi M, et al. Pulsed Electric Field Treatment Enhances the Cytotoxicity of Plasma-Activated Liquids in a Three-Dimensional Human Colorectal Cancer Cell Model. *Sci Rep* (2019) 9:7583. doi:10.1038/s41598-019-44087-5
51. García D, Gómez N, Mañas P, Condón S, Raso J, Pagán R. Occurrence of Sublethal Injury after Pulsed Electric fields Depending on the Micro-organism,

the Treatment Medium Ph and the Intensity of the Treatment Investigated. *J Appl Microbiol* (2005) 99(1):94–104. doi:10.1111/j.1365-2672.2005.02611.x

52. Pastorek M, Suchoňová M, Konečná B, Pásztor S, Petrus J, Ivašková N, et al. The Effect of Air Plasma Activated Liquid on Uropathogenic Bacteria. *Plasma Chem Plasma Process* (2022) 42(3):561–74. doi:10.1007/s11090-022-10239-1
53. Janda M, Martišovitš V, Machala Z. Transient Spark: a Dc-Driven Repetitively Pulsed Discharge and its Control by Electric Circuit Parameters. *Plasma Sourc Sci. Technol.* (2011) 20:035015. doi:10.1088/0963-0252/20/3/035015
54. Janda M, Machala Z, Niklová A, Martišovitš V. The Streamer-To-Spark Transition in a Transient Spark: a Dc-Driven Nanosecond-Pulsed Discharge in Atmospheric Air. *Plasma Sourc Sci. Technol.* (2012) 21:045006. doi:10.1088/0963-0252/21/4/045006
55. Tarabová B, Lukeš P, Hammer MU, Jablonowski H, von Woedtke T, Reuter S, et al. Fluorescence Measurements of Peroxynitrite/peroxynitrous Acid in Cold Air Plasma Treated Aqueous Solutions. *Phys Chem Chem Phys* (2019) 21(17): 8883–96. doi:10.1039/c9cp00871c
56. Eisenberg G. Colorimetric Determination of Hydrogen Peroxide. *Ind Eng Chem Anal Ed* (1943) 15(5):327–8. doi:10.1021/i560117a011
57. Lukes P, Locke BR, Brisset JL. Aqueous-Phase Chemistry of Electrical Discharge Plasma in Water and in Gas-Liquid Environments. *Plasma Chem Catal Gases Liquid* (2012)(7) 243–308. doi:10.1002/9783527649525.CH7
58. Pillet F, Formosa-Dague C, Baaziz H, Dague E, Rols M-P. Cell wall as a Target for Bacteria Inactivation by Pulsed Electric fields. *Sci Rep* (2016) 6:19778. doi:10.1038/srep19778
59. Song J, Joshi RP. Temperature Effects on High-Intensity, Ultrashort Electric Pulse Induced Cell Death. 2014 40th Annual Northeast Bioengineering Conference (NEBEC) (2014). doi:10.1109/NEBEC.2014.6972944
60. Joshi R. Synergy Between Electric Pulse and Thermal Effects. *Ultrashort Electric Pulse Effects Biol Med* (2021) 301–15. doi:10.1007/978-981-10-5113-5_1310.1007/978-981-10-5113-5_12
61. Hohnholt MC, Blumrich EM, Dringen R. Multiassay Analysis of the Toxic Potential of Hydrogen Peroxide on Cultured Neurons. *J Neurosci Res* (2014) 93:1127–37. doi:10.1002/jnr.23502
62. Trosset J-Y, Carbonell P. Synergistic Synthetic Biology: Units in Concert. *Front Bioeng Biotechnol* (2013) 1:1–11. doi:10.3389/fbioe.2013.00011
63. Traylor MJ, Pavlovich MJ, Karim S, Hait P, Sakiyama Y, Clark DS, et al. Long-term Antibacterial Efficacy of Air Plasma-Activated Water. *J Phys D: Appl Phys* (2011) 44:472001. doi:10.1088/0022-3727/44/47/472001
64. Lukes P, Clupek M, Babicky V, Vykouk T. Bacterial Inactivation by Pulsed corona Discharge in Water. 16th IEEE International Pulsed Power Conference (2007). doi:10.1109/PPPS.2007.4651849

Conflict of Interest: The authors declare that the research was conducted in the absence of any commercial or financial relationships that could be construed as a potential conflict of interest.

Publisher's Note: All claims expressed in this article are solely those of the authors and do not necessarily represent those of their affiliated organizations, or those of the publisher, the editors, and the reviewers. Any product that may be evaluated in this article, or claim that may be made by its manufacturer, is not guaranteed or endorsed by the publisher.